JOURNAL OF NANO- AND ELECTRONIC PHYSICS
Vol. **10** No 3, 03029(6pp) (2018)

ЖУРНАЛ НАНО- ТА ЕЛЕКТРОННОЇ ФІЗИКИ
Том **10** № 3, 03029(6cc) (2018)

Ultrafine β - FeOOH: the Influence of Synthesis Conditions on the Morphological, Magnetic and Electrochemical Properties

L.V. Mokhnatska[1], V.O. Kotsyubynsky[1], A.B. Hrubiak[2], S.V. Fedorchenko[1], S.I. Vorobiov[3]

[1] *Vasyl Stefanyk Precarpathian National University, 57, Shevchenko Str., 76025 Ivano-Frankivsk, Ukraine*
[2] *Institute of Metal Physics, National Academy of Science, 36, Acad. Vernadsky Str., 03680 Kyiv, Ukraine*
[3] *Sumy State University, 2, Rymskyi-Korsakov Str., 40007 Sumy, Ukraine*

(Received 25 October 2017; published online 25 June 2018)

Ultrafine sol-gel synthesized iron oxy-hydroxides β-FeOOH was investigated by XRD, TEM, Mossbauer and impedance spectroscopies and low temperature nitrogen adsorption. The influence of precursor molar concentration on the material morphology, crystalline and magnetic microstructures was studied. The model of initial precursors ($FeCl_3 \cdot 6H_2O$) molarity influence on the mesoporous β-FeOOH formation is proposed. The electrochemistry performance of obtained materials in aqueous electrolyte (1 M Li_2SO_4) was tested and lithium ions diffusion coefficients were calculated. The work is aimed to identify the optimal conditions for obtaining the perspective electrode material for supercapacitors.

Keywords: Iron oxy-hydroxide, β-FeOOH, Crystal and magnetic structure, Morphology, CVA.

DOI: 10.21272/jnep.10(3).03029 PACS numbers: 68.37.Lp, 61.05.C, 82.45.Yz

1. INTRODUCTION

Iron oxides and oxy-hydroxides in particular akaganeite β-FeOOH have a great scientific and technological interest due to its low cost and good stability as pigments, catalysts, sorbents and ion-exchange material [1]. The transition to ultrafine materials allows using size-related properties and expanding the application sphere. Superparamagnetic iron oxides and oxy-hydroxides nanoparticles have been used for magnetic resonance imaging contrast enhancement, tissue repair, detoxification of biological fluids, hyperthermia, and drug delivery [2]. Akaganeite with high specific surface area is an outstanding adsorbent for removal of various pollutants [3]. Channel-type structure of β-FeOOH is suitable for reversible intercalation of lithium ion with theoretical discharge capacity about 302 mAh·g^{-1}. Ultrafine β-FeOOH first approbation as a positive material for lithium secondary cells demonstrates good lithium intercalation reversibility with a capacity of about 275 mA·h/g [4]. There are several reports on β-FeOOH, e.g. about very high capacitance up to 1400 mAh·g^{-1} [5], which is caused by a series of reactions intercalation and conversion, formation/deformation of solid-state electrolyte interface layers and interfacial storage. As a result ultrafine beta-iron oxy-hydroxide is a promising electrode material for high-performance hybrid supercapacitor with the storage mechanism charge via rapid redox reactions on the electrode/electrolyte boundaries [6]. In view of these applications the obtaining of iron oxy-hydroxide materials with mesoporous structure and controlled morphology has a great significance.

In this paper we investigate the influence of synthesis conditions on the structural, morphological and magnetic properties of ultrafine akaganeite and test electrochemical performance of these materials in aqueous electrolyte.

2. EXPERIMENTAL DETAILS

The iron hydroxides β-FeOOH with tunnel structure and rod-like morphology was synthesized by controlled hydrolysis and precipitation. In a typical synthesis, 1 M aqueous NaOH was added dropwise into aqueous $FeCl_3$ at 55-65 °C with vigorous stirring. Obtained colloidal solutions were kept at 65 °C for 24 h. The precipitates were collected and washed with deionized water several times and finally dried at 100°C overnight. Three systems (F1, F2 and F3) were obtained at different $FeCl_3 \cdot 6H_2O$ molar concentration in the initial solution (0.1 M, 0.37 M and 0.55 M, respectively).

Diffraction patterns were obtained with DRON-4-07 diffractometer (Cu Kα radiation). Bragg-Brentano geometry and a Ni Kβ-filter were used. A qualitative analysis was carried out through ICSD structural models. The structural model for β-FeOOH was based on the ICSD records #36400. Annealing at vacuum (850-900 °C for 4 h) of copper powder with an average grain size of about 50 μm was used as reference sample for the determination of the instrumental peak broadening. The size of the coherently scattering domains was calculated by the Scherrer equation: $D = \frac{K\lambda}{\beta \cos\theta}$, where K is the Scherrer constant ($K = 0.9$), λ is the wavelength (0.15405 nm), β is the FWHM (in radians) and θ is the peak angular position. Pseudo-Voight was used for profile shape modeling.

The Mössbauer spectra were measured with a MS-1104Em spectrometer using a ^{57}Co γ-ray source and calibrated at room temperature with α-Fe as a standard (line width 0.29 mm/s). The isomer shifts (δ) are relative to Fe metal. The fitting was performed using UnivemMs 701 software.

The specific surface area and pore size distribution were measured by nitrogen adsorption at 77.2 K (Quantachrome NOVA 2200e porosimeter). Before taking measurements, the samples were degassed at 150 °C for 6-8 h. The specific surface area was determined by the multipoint BET method. Pore size distribution was determined by BJH method [7].

Electrochemical process at the electrode / electrolyte

interface was investigated by cyclic voltammetry method using AUTOLAB Autolab PG-STAT 12/FRA-2 frequency. Experiments were carried by using standard three-electrode scheme. The electrolyte was aqueous 1 M Li_2SO_4, platinum and silver chloride electrode was used as the counter and reference electrodes, respectively a powder electrode. The plate powder electrodes (area about 1.5 cm^2, thickness 0.05 cm) were prepared by nickel grid covering by paste on the base of synthesized materials including 10 mass % of C.

3. RESULTS AND DISCUSSION

All samples were monophase β-FeOOH (Fig.1). The increasing of iron-containing precursors causes the decrease of material crystallinity: the average sizes of coherent scattering domains (CSD) for F1 sample are about 15-20 nm, F2 – 5-6 nm calculated from XRD reflexes broadening. At the same time F3 sample is close to amorphous.

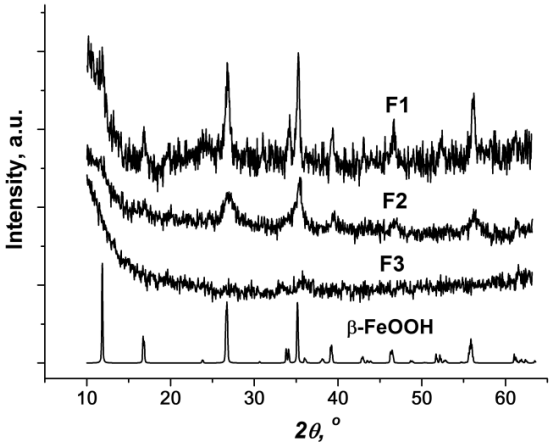

Fig. 1. – XRD patterns of β-FeOOH obtained at different $FeCl_3 \cdot 6H_2O$ molar concentration

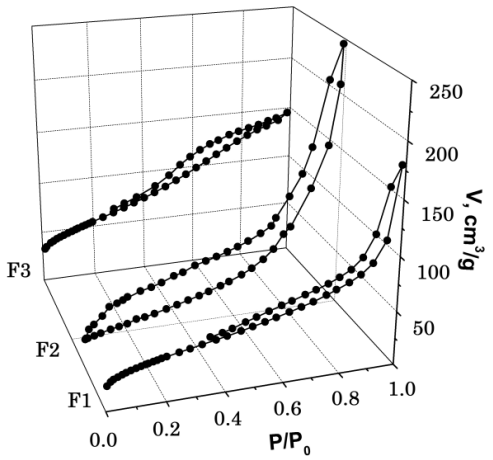

Fig. 2. – Adsorption/desorption isotherms of β-FeOOH obtained at different $FeCl_3$ molarity

Morphological differences between samples were observed by adsorption porosimetry method. The adsorption isotherm patterns of obtained samples and correspondent pores size distribution patterns are presented in Fig. 2 and 3, respectively.

The continuous pore sizes distribution range from micropore to mesopore is observed for F1 sample. Mesopore size distribution for F1 sample is uniform in the 2-25 nm range and micropore fraction is present. However, when $FeCl_3 \cdot 6H_2O$ molarity increases to 0.37 M volume adsorbed at low P/P0 is low and total porosity is less with preferential reduction in mesoporosity, which indicates pore shrinkage. Low-pressure hysteresis for this sample may be associated with the change in volume of the adsorbent for example, the swelling of non-rigid pores.

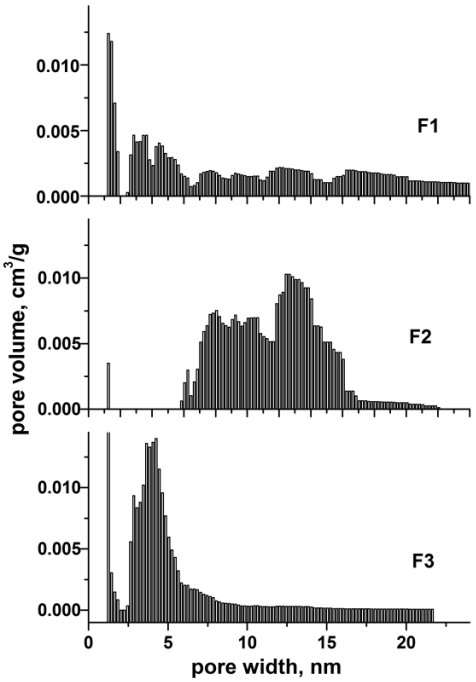

Fig. 3 – Pore size distribution patterns of β-FeOOH obtained at different $FeCl_3$ molarity

Microporosity is absent for F2 and a fraction of mesopores is retained for 6-16 nm range. The adsorbtion at high P/P0 (>0.8) is the maximal for this sample – up to 265 cm^3/g which is due to dehydroxylation as well as the possible structural change. F3 sample is characterized the narrow mesopore distribution in a range 2-10 nm with the micropore presence (up to 10 %). Therefore, the adsorption of isotherm shows a perfect Type V behavior accordingly to empirical classification of hysteresis loops given by IUPAC and H4 type hysteresis associated with narrow slit pores [8]. The specific surface areas for F1, F2 and F3 systems were 138, 143 and 190 m^2/g, respectively. The F3 sample is paracrystalline and exhibit a relatively narrow distribution of pores only in the mesoporous range. [9].

The effect of concentration on the size and morphology of particles is shown in Fig. 4: F1 sample consists of ellipsoidal agglomerates with the sizes about 40x200 nm. Agglomerates were observed for F3 sample too. At the same time F2 sample is characterized by separate particles with the average sizes not more than 30 nm. This result is confirmed by Mössbauer method.

Mössbauer spectra of all β-FeOOH samples are characterized by presence of a dominating doublet component correspond to absorption by the nucleus of tetrahedral coordinated ions Fe^{3+} in the high-spin state (Fig. 5).

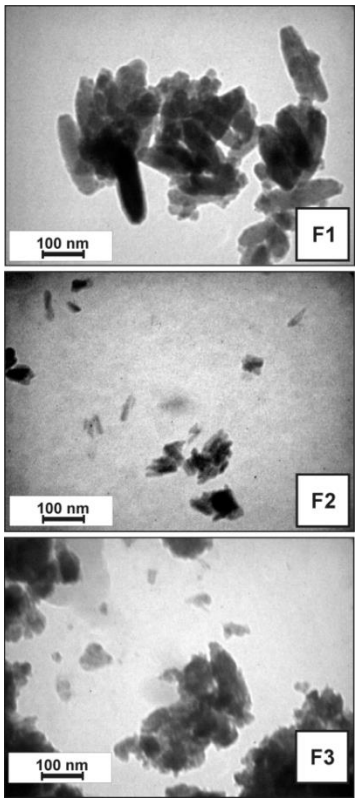

Fig. 4 – TEM images of samples (F1, F2 and F3)

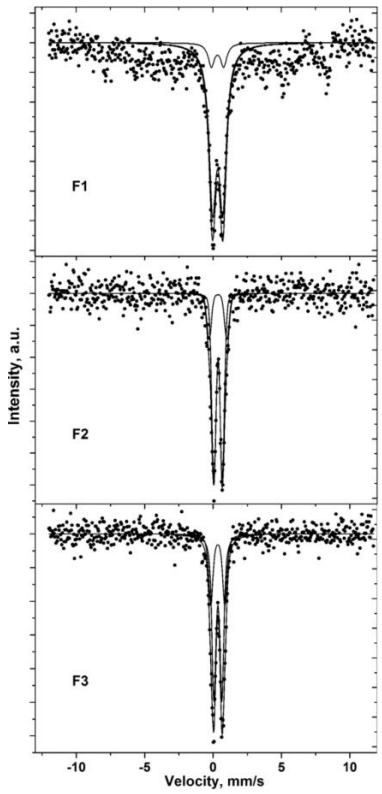

Fig. 5 – Mossbauer spectra β-FeOOH obtained at different $FeCl_3 \cdot 6H_2O$ molar concentration

The formation of doublet component is the result of sizes effects and superparamagnetism phenomena [10]. The obtained materials can be represented as systems of monodomain clusters with fluctuated magnetic moments. For particles with uniaxial magnetic anisotropy the relaxation time τ_r of magnetic moments was calculated accordingly to relationship : $\tau_r = \tau_0 \exp\left(\frac{KV}{kT}\right)$, where $\tau_0 \approx 10^{-9}$ s, V – wave rage volume of the particle, K – constant of magneto-crystalline uniaxial anisotropy, T – blocking temperature. At the relaxation time τ_r less the ^{57}Co excited state lifetime (about 10^{-7} s) the particle became paramagnetic. The fluctuations cause the disappearance of magnetic hyperfine splitting at certain combination of V, K and T parameters. The constant of magneto-crystalline anisotropy K of β-FeOOH with fine particles was about $2.1 \cdot 10^3$ J/m^3 [11]. For spectra obtained at room temperature (293 K) the transition from magnetically ordered state to superparamagnetic will occurred for particles with the sizes less than 15 nm (spherical approach) due comparatively low values of magneto-crystalline anisotropy. This result agrees with XRD data about average sizes of CSR.

All experimental spectra are the superposition of the two doublets with close isomeric shift δ_s (about 0.35-0.37 mm/s) and different quadrupole splitting Δ (tab.1, fig.5). The increasing of quadrupole splitting for minor component in a range 0.91-1.31 mm/s was observed at the close values of quadrupole splitting for dominant component.

Table 1 – Parameters of Mossbauer Spectra for Synthesized Materials

Sample	δ_s, mm/s	Δ_s, mm/s	ω, mm/s	S, %
F1	0.353	0.583	0.35	83.5
	0.364	1.102	0.37	16.5
F2	0.348	0.641	0.52	77.9
	0.333	0.908	0.45	22.1
F3	0.368	0.620	0.38	68.1
	0.362	1.311	0.41	31.9

The presence of two doublets caused by the difference in near surroundings of ^{57}Fe nuclei located in non-equivalent crystal positions in the inner and outer parts of sintered β-FeOOH particles which form mesoporous grid [12].The ratio between relative areas of these two doublets depends on the precursor molar concentration for all samples and it is minimal for F1 sample. Only for F1 sample it has very broad magnetic component of Mossbauer spectra so the average particle size is close to 15-20 nm.

We can suggest the following model of precursor's molarity impact on of iron oxy-hydroxides nucleation. The first stage of the material synthesis involves the $FeCl_3 \cdot 6H_2O$ salts hydrolysis and $[Ti(OH_2)_6]^{4+}$ monomers formation where Fe^{3+} ions are in the octahedral coordination[13]. Applying the partial charge theory [14], the hydrolysis ratio h for monomers $[Fe(OH)_h(OH_2)_{6-h}]^{(4-h)+}$ as a function of pH was calculated. The hydrolysis products are monomers $[Fe(OH)(OH_2)_5]^{3+}$ when the pH of the reaction medium is less 2. If the pH is about 4 and 7 the hydrolysis leads to the formation of the $[Fe(OH)_2(OH_2)_4]^{2+}$ and $[Fe(OH)_3(OH_2)_3]^{+}$ complexes, respectively. For pH > 8 the sol consists of $[Fe(OH)_4(OH_2)_2]^{0}$ monomers and the conditions of sol

stability are violated. The aqueous NaOH solution as a pH regulator was used in our case (final pH was 8.5-9.0). At this stage the formation of the iron hydroxypolymers due olation interaction between hydrocomplexes will happen. Bridges formation during oxolation reaction ends with β-FeOOH structure develops [15]. The tendency to average particle sizes decreasing with the enlarging of precursor's molar concentration can be explained by the peculiarities of a gel formation. Slow aggregation regime leads to enlarging the quantity of interacting clusters and particles (reaction limited cluster aggregation mechanism is dominated). The increasing of molar concentration at these conditions causes the sizes decreasing of primary clusters at the gel formation stage [16]. The decomposition of metal-organic precursor during the dried gel annealing leads to mesoporous iron oxide formation with morphological properties depending on the precursor's concentration.

CVA technique allows to obtain the information about the kinetics of the electrode process and mass transport through electrode/electrolyte (1 M aqueous Li_2SO_4) interface (Fig. 6). The simplest system involves a quasi-reversible redox reaction with single-electron transfer. The charge-discharge reaction for β-FeOOH is one electron transfer: β-FeOOH + Li^+ + e^- ↔ LiFeOOH, where Fe(III) is reduced to Fe(II) during discharge and Fe(II) is reoxidized to Fe(III) during charge. The reaction allow estimate about one lithium ion reversibly intercalate/deintercalate into/from β-FeOOH structure per formula unit.

There are several stages of the lithium-ion intercalation reaction near electrode/lectrolyte interface: lithium-ion diffusion transfer in the electrolyte, Li^+-ion transfer through electrolyte/electrode interface and Li^+-ion insertion and extraction through active materials. CV curves (Fig. 6) are characterized of a pair of weak redox peaks indicating the capacitance are induced both by Faradaic redox reactions and electric double layer formation.

The increasing of scan rates leads to the oxidation and reduction peaks shifting to more positive or negative potentials, respectively. This indicates increasing of the electrode internal resistance during cycling. The specific capacitance of the electrode was calculated from the CV curves as $C = \frac{\Delta Q}{\Delta U \cdot m}$ were $\Delta Q = \frac{1}{\nu}\int_{U_1}^{U_2} I(U)\,dU$, where C – specific capacitance (F/g), I - current density (A/cm^2), V_1 and V_2 is the potential window (V), ν - potential scan rate (mV/s), m – mass of the electroactive materials (g/cm^2).

The capacitance of the β-FeOOH electrode increases with the enlarging of material specific surface area (Fig. 7). A highest specific capacitance of F2 can be obtained at 1 mV/s − 1 for the F2. When the scan rate is increased to 50 mV/s the specific capacitance of these electrode drops to F/g (retain 15 % of its initial value). For all systems the specific capacitance decreases with the scan rate increasing which is caused by the electrolyte ions diffusion limiting at high scan rates.

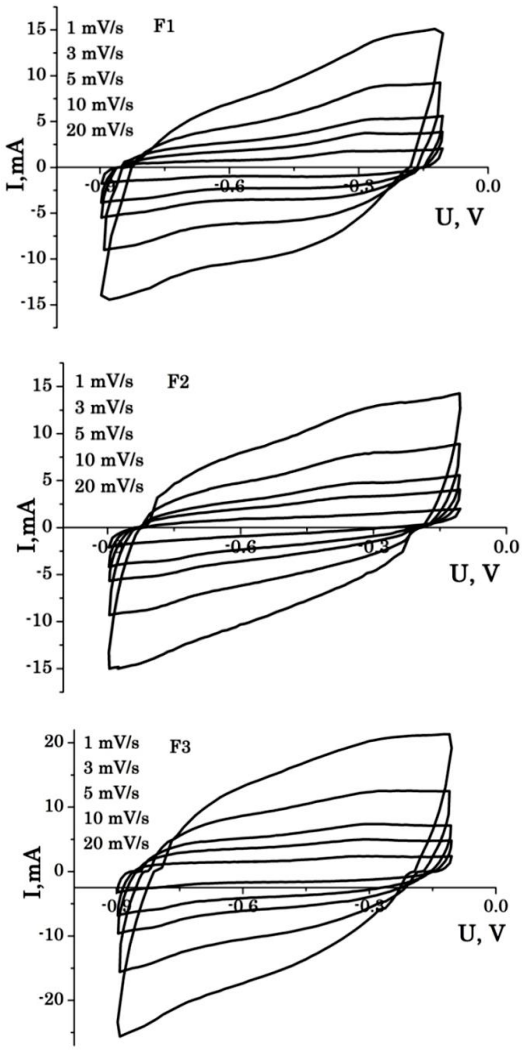

Fig. 6 – Cyclic voltammograms at sweep rates 1, 3, 5, 10, 20 mV/s for β-FeOOH based electrode (1M Li_2SO_4 aqueous solution) spectra β-FeOOH obtained at different $FeCl_3 \cdot 6H_2O$ molar concentration

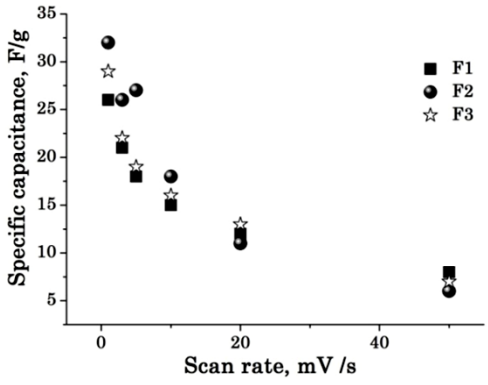

Fig. 7 – Specific capacitance of β-FeOOH electrode as a function of the scan rates based on the CV curves (1M Li_2SO_4 aqueous solution) spectra β-FeOOH obtained at different $FeCl_3$ $6H_2O$ molar concentration

CVA curves at low scan rates are characterized by redox peaks at 0.60-0.65 V which associated with reversible Li^+ ions intercalation. The reduction peaks shift negatively and the oxidation peaks shift positively

with the scan rate increasing. The diffusion coefficient (D) was calculated from the CVA data using linear approximation of i_p vs $\nu^{1/2}$ plot [17]: $i_p = 2.99\times10^5(\alpha n)^{1/2} A\Delta C D_{Li}^{1/2}\nu^{1/2}$ (where i_p – peak current, ν – scan rate, A – the electrode area, α – transfer coefficient, C – Li-ion molar concentration in electrode, n – number of electrons transferred in the redox process (n = 1), F – Faraday constant, R – gas constant, T – temperature. The obtained value of diffusion coefficient is in a range (1.0-3.0) $\cdot10^{-13}$ cm$^2\cdot$s^{-1}. This result indicates the 3D-arrangement of intercalated ions during the intercalation.

4. CONCLUSION

The variation of precursor's ($FeCl_3\cdot6H_2O$) molar concentration during ultrafine β-FeOOH sol-gel synthesis allow to obtain the mesoporous superparamagnetic materials. The growth of precursor's molarity from 0.10 M to 0.55 M leads to average particle sizes decreasing and enlarging BET specific surface area in a range 138-190 m^2/g. The pore size distributions and mesopore relative content depend on the precursor's molarity. The synthesized materials can be represented as systems of monodomain clusters with fluctuated magnetic moments. The obtained results are probably caused by transitions from diffusion limited aggregation reaction to limited cluster slow aggregation. The specific capacitances of β-FeOOH samples (calculated from the CVA data) are about 26-29 F/g. Li^+ ions diffusion coefficient slightly depends on the scan rate and changes in a the range of (1.0-3.0) $\cdot10^{-13}$ cm$^2\cdot$s^{-1}.

Ультрадисперсный β-FeOOH: влияние условий синтеза на морфологические, магнитные и электрохимические свойства

Л.В. Мохнацкая[1], В.О. Коцюбинский[1], А.Б. Грубяк[2], Федорченко С.В.[1], С.І. Воробьёв[3]

[1] *ДВНЗ "Прикарпатский национальный университет имени Василия Стефаныка", ул. Шевченко, 57, 76025 Ивано-Франковск, Украина*

[2] *Институт металлофизики им. Г.В. Курдюмова НАН Украины, ул. Акад. Вернадского, 36, 03680 Киев, Украина*

[3] *Сумский государственный университет, ул. Римского-Корсакова, 2, 40007 Сумы, Украина*

Ультрадисперсный оксигидрооксид железа β-FeOOH, синтезированный золь-гель методом, исследовали с помощью рентгеновской, ТЕМ, Мессбауэровской и импедансной спектроскопии и низкотемпературной адсорбции азота. Изучено влияние молярной концентрации прекурсоров на морфологию, кристаллическую и магнитную микроструктуры материала. Предложена модель влияния молярности выходных прекурсоров ($FeCl_3\cdot6H_2O$) на формирование мезопористости β-FeOOH. Проведено электрохимические исследования полученных материалов в водном электролите (1 M Li_2SO_4) и рассчитаны коэффициенты диффузии ионов лития. Работа направлена на определение оптимальных условий для получения перспективного материала для электродов суперконденсаторов.

Ключевые слова: Оксигидрооксид железа, β-FeOOH, Кристаллическая и магнитная структура, Морфология, Циклическая вольтамперометрия.

Ультрадисперсний β-FeOOH: вплив умов синтезу на морфологічні, магнітні та електрохімічні властивості

Л.В. Мохнацька[1], В.О. Коцюбинський[1], А.Б. Грубяк[2], Федорченко С.В.[1], С.І. Воробйов[3]

[1] *ДВНЗ "Прикарпатський національний університет імені Василя Стефаника", вул. Шевченка, 57, 76025 Івано-Франківськ, Україна*

[2] *Інститут металофізики ім. Г.В. Курдюмова НАН України, вул. Акад. Вернадського, 36, 03680 Київ, Україна*

[3] *Сумський державний університет, вул. Римського-Корсакова, 2, 40007 Суми, Україна*

Ультрадисперсний оксигідрооксид заліза β-FeOOH, синтезований золь-гель методом, досліджували за допомогою рентгенівської, ТЕМ, Месбауерівської та імпедансних спектроскопії та низькотемпературної адсорбції азоту. Вивчено вплив молярної концентрації прекурсорів на морфологію, кристалічну та магнітну мікроструктури матеріалу. Запропоновано модель впливу молярності вихідних прекурсорів ($FeCl_3\cdot6H_2O$) на формування мезопористості β-FeOOH. Проведено електрохімічні дослідження отриманих матеріалів у водному електроліті (1 M Li_2SO_4) та розраховано коефіцієнти дифузії іонів літію. Робота спрямована на визначення оптимальних умов для одержання перспективного матеріалу для електродів суперконденсаторів.

Ключові слова: Оксигідрооксид заліза, β-FeOOH, Кристалічна та магнітна структура, Морфологія, Циклічна вольтамперометрія.

REFERENCES

1. M. Mohapatra, S. Anand, *Int. J. Eng., Sci. Technol.* **2** No8, 127 (2010).
2. A.K. Gupta, M. Gupta, *Biomaterials* **26** No 18, 3995 (2005).
3. J. Zhao, W. Lin, Q. Chang, W. Li, Y. Lai, *Environmental Technol. Rev.* **1** No 1, 114 (2012).
4. K. Amine, H. Yasuda, M. Yamachi, *J. Power Source.* **81**, 221 (1999).
5. L. Yu, S. Xi, C. Wei, W. Zhang, Y. Du, Q. Yan, Z. Xu, *Adv. Energy Mater.* **5** No 6 1401517 (2015).
6. Wei-Hong Jin, Gen-Ting Cao, Jing-Ya Sun, *J. Power Source.* **175** No 1, 686 (2008).
7. S. Storck, H. Bretinger, W.F. Maier, *Appl. Catalysis A: General* **174** No 1 137 (1998).
8. J.E. Shields, S. Lowell, M.A. Thomas, M. Thommes, *Fundamental Aspects of Silicate Mesoporous Materials* 43 (2004).
9. A. Galarneau, F. Villemot, J. Rodriguez, F. Fajula, B. Coasne, *Langmuir* **30** No 44, 13266 (2014).
10. L.Y. Zhang, J. Feng, D.S. Xue, *Mater. Lett.* **61** No 6 1363 (2007).
11. J. Takagi, M. Ozaki, K. Shigemasa, T. Mizoguchi, *Mater. Trans.* **51** No 7 1330 (2010).
12. V. Kotsyubynsky, B. Ostafiychuk, V. Moklyak, A. Hrubiak. *Solid State Phenomena* **230**, 120 (2015).
13. V.O. Kotsyubynsky, I.F. Myronyuk, L.I. Myronyuk, V.L. Chelyadyn, M.H. Mizilevska, A.B. Hrubiak, F.M. Nizamutdinov, *Materialwissenschaft und werkstofftechnik* **47** No2-3, 288 (2016).
14. M. Henry, J. P. Jolivet, J. Livage, *Struct. Bonding* **77**, 153 (1992).
15. S. Musić, A. Vertes, G. W. Simmons, I. Czakó-Nagy, H. Leidheiser, *J. Colloid Interface Sci.* **85** No 1, 256 (1982).
16. J. Primera, A. Hasmy, T. Woignier, *J. Sol-Gel Sci. Technol.* **26**, 671 (2003).
17. P. He, X. Zhang, Y. G. Wang, L. Cheng, Y. Y. Xia, *J. Electrochem. Soc.* **155** No 2 155, A144 (2008).